Inorganic Chemistry

Article

pubs.acs.org/IC

Synthesis of $(TDAE)(O_2SSO_2)(s)$ and Discovery of $(TDAE)(O_2SSSSO_2)(s)$ Containing the First Polythionite, $[O_2SSSSO_2]^{2-}$

Pablo Bruna,[†] Andreas Decken,[†] Scott Greer,[†] Friedrich Grein,[†] H. Donald B. Jenkins,[‡] Birgit Mueller,[†] Jack Passmore,*[,†] Tressia A. P. Paulose,[†] J. Mikko Rautiainen,[§] Stephanie Richardson,[†] and Melbourne J. Schriver[∥]

[†]Department of Chemistry, University of New Brunswick, P.O. Box 4400, Fredericton, New Brunswick E3B 5A3, Canada

[‡]Department of Chemistry, University of Warwick, Gibbet Hill, Coventry, West Midlands, CV4 7AL United Kingdom

[§]Department of Chemistry, University of Oulu, P.O. Box 3000, 90014 Oulu, Finland

[∥]Department of Chemistry, Crandall University, P.O. Box 6004, Moncton, New Brunswick, E1C 9L7, Canada

Supporting Information

ABSTRACT: Gaseous SO_2 reacts with tetrakis(dimethylamino)-ethylene (TDAE) in acetonitrile in a 2:1 stoichiometric ratio to give analytically pure insoluble purple $(TDAE)(O_2SSO_2)$ (**1**) in about 80% yield. Crystals of $(TDAE)(O_2SSSSO_2)$ (**2**) were obtained from orange solution over the purple solid. The Raman spectrum of $[TDAE]^{2+}$ was established using (TDAE)(A) salts [A = $2Br^-$, $2Br^-\cdot 2H_2O$ (X-ray), $2[Br_3]^-$ (X-ray)]. Vibrational spectroscopy showed that $[O_2SSO_2]^{2-}$ in **1** has C_{2h} geometry. The X-ray structure of **2** showed that it contained $[O_2SSSSO_2]^{2-}$, the first example of a new class of sulfur oxyanions, the polythionites. The geometry of $[O_2SSSSO_2]^{2-}$ consists of S_2 with an S–S bond length of 2.003(1) Å connected to two terminal SO_2 moieties by much longer S–S bonds of 2.337(1) Å. Calculations (B3PW91/6-311+G(3df)) show that the structural units in $[O_2SSSSO_2]^{2-}$ are joined by the interaction of electrons in two mutually perpendicular π^* SOMOs of the triplet-state diradical S_2 with unpaired electrons in the π^*-antibonding orbitals of the two terminal $[SO_2]^{\bullet-}$ and polarized to delocalize the negative charge equally onto the three fragments. Thermodynamic estimates show **2** to be stable with respect to loss of sulfur and formation of **1**, in contrast to $[O_2SSSSO_2]^{2-}$ salts of small cations that are unstable toward the related dissociation. Reaction of TDAE with an excess of liquid SO_2 led to $(TDAE)(O_3SOSO_3)\cdot SO_2$ (preliminary X-ray, Raman), $(TDAE)(O_3SSSSO_3)\cdot 2SO_2$ (preliminary X-ray, Raman), and $(TDAE)(O_3SSO_2)$ (Raman).

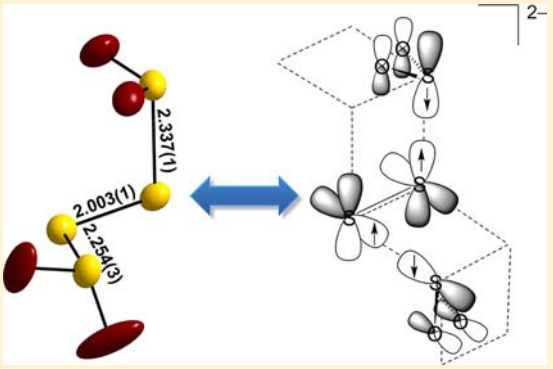

1. INTRODUCTION

Dithionite salts have been of industrial and scientific importance[1] since their discovery in the 19th century.[2] The structure of dithionite was contentious until 1956, when Dunitz determined the X-ray structure of $Na_2(O_2SSO_2)$,[3] showing that $[O_2SSO_2]^{2-}$ had a cis C_{2v} eclipsed structure with a very long S–S bond (2.389(8) Å, cf. S–S (S_8) 2.055(2) Å).[4] Subsequently, very similar structures were found in $Sn_2(O_2SSO_2)_2$[5] and $Zn(O_2SSO_2)$[6] and a related gauche C_2 structure with an S–S bond of 2.298(4) Å in $Na_2(O_2SSO_2)\cdot 2H_2O$ and a second form of $Na_2(O_2SSO_2)$ with a nearly eclipsed $[O_2SSO_2]^{2-}$ structure and with an S–S distance of 2.392(2) Å.[7] In the solid state $[O_2SSO_2]^{2-}$ can be regarded as containing two $[SO_2]^{\bullet-}$ radical anions joined by a very long and weak S–S bond. In the gas phase $[O_2SSO_2]^{2-}$ is unstable with respect to dissociation into two $[SO_2]^{\bullet-}$ radical anions [MP2/6-311+G(2d,p) −271 kJ mol^{-1}].[8] We anticipated that the chemical reactivity of dithionite would be increased on reduction of lattice energies of salts of large cations, relative to those of salts of the well-known small cations. Of particular interest to us was the development of dithionite salts of large cations for SO_2 absorption.[9] There were two such salts in the literature, $(NEt_4)_2(O_2SSO_2)$[10] and [18-crown-6 $Na]_2(O_2SSO_2)$.[11] However, we showed that although [18-crown-6 $Na]_2(O_2SSO_2)$ is formed in methanol, it dissociates to $Na_2(O_2SSO_2)(s)$ and 18-crown-6(s) in the solid state, driven by the large lattice energy of $Na_2(O_2SSO_2)(s)$ relative to that of [18-crown-6 $Na]_2(O_2SSO_2)$.[12] $(NEt_4)_2(O_2SSO_2)$ has been characterized by C, H, and N (but not S) elemental analyses and by vibrational spectroscopy that showed $[O_2SSO_2]^{2-}$ to have a C_{2h} trans conformation.[13] Literature preparation of $(NEt_4)_2(O_2SSO_2)$ employed ion-exchange methods in aqueous solution using commercially available but impure $Na_2(O_2SSO_2)$.[10] In our hands, preparation of this and other tetraalkylammonium dithionite salts in high purity was not trivial.[9b,14]

A potential simple one-step route to a desired large cation dithionite salt is reaction of the organic electron donor, liquid

Received: August 30, 2013
Published: November 15, 2013

   dx.doi.org/10.1021/ic4022195 | Inorg. Chem. 2013, 52, 13651–13662

Scheme 1. Born–Fajans–Haber Cycle [kJ mol^{-1}] for Reaction of TDAE with 2 Mol Equiv of SO_2[a]

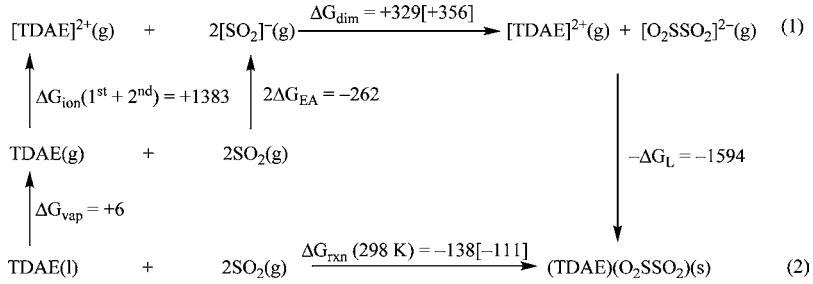

[a]Electron affinities, ionization energies, and gas-phase dimerization energies have been estimated with the B3PW91/6-311+G(3df) [B3PW91/6-31G(d)] method. For details of the lattice energy calculations see Supporting Information Section S3 and ΔG_{vap}(298 K) of TDAE ref 17.

tetrakis(dimethylamino)ethylene (TDAE),[15] and gaseous SO_2, an electron acceptor. We estimated this reaction to be favorable (Scheme 1, details have been given in Section S3 in the Supporting Information) using good-level DFT calculations for gas-phase energies and volume-based thermodynamics for lattice energies (VBT)[16] of the as yet unknown salts. Results are presented in Scheme 1.

2. RESULTS AND DISCUSSION

2.1. Reaction of TDAE(l) with $2SO_2$(g) Leading to Analytically Pure 1 and Crystals of 2. A 2 mol equiv amount of sulfur dioxide gas was expanded into a vessel containing liquid TDAE with absorption of the gas, resulting in formation of a purple solid and evolution of significant amounts of heat. To control heat formation the reaction was modulated by carrying it out in acetonitrile solution leading to insoluble purple, analytically pure (H, C, N, and S) **1** in 80% yield according to eq 3, as predicted by our thermodynamic

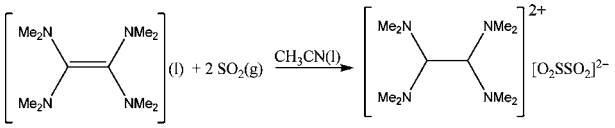

(3)

calculations. We note that the alternative salt $[TDAE]^+[O_2SSO_2]^-$(s) was not formed as it is thermodynamically unstable with respect to $[TDAE]^{2+}[O_2SSO_2]^{2-}$(s) ($\Delta H_{rxn}$ = −162 and ΔG_{rxn}(298 K) = −148 kJ mol^{-1}; see Supporting Information Section S3.6 for details). While most dithionite salts are colorless, there have been reports of yellow $(NEt_4)_2(O_2SSO_2)$[10] and colored complexes[18] of the dithionite anion. Preliminary TDDFT calculations on model ion pair systems suggest that the purple color of **1** could be related to a charge-transfer transition from the $[O_2SSO_2]^{2-}$ dianion to low-lying orbitals of the $[TDAE]^{2+}$ dication, while in metal dithionite salts the corresponding transition would be at higher energies (see Supporting Information Section S3.1 for details).

In addition to purple solid, reaction 3 gave an orange solution, from which, over time, a white $(TDAE)(O_3SSO_2)$(s) powder (Raman analysis see Supporting Information, Section S2.6.1, Figure S20, and Table S4) and crystals of orange **2** were obtained (Scheme 2).

The presence of **2** and $(TDAE)(O_3SSO_2)$ may be envisaged as arising according to eq 4 via soluble unidentified intermediate species in the orange solution.

$$5\text{TDAE(l)} + 12\text{SO}_2(g) \rightarrow 4(\text{TDAE})(\text{O}_3\text{SSO}_2)(\text{s}) + (\text{TDAE})(\text{O}_2\text{SSSSO}_2)(\text{s}) \quad (4)$$

Reactions of distilled TDAE(l) and SO_2(g) in liquid propionitrile gave **1** but no orange **2**.[9b] Reaction of TDAE(l) with an excess of liquid SO_2 gave after some time (TDAE)(A) (A = $[O_3SSSSO_3]^{2-}$, $[O_3SOSO_3]^{2-}$, and $[O_3SSO_2]^{2-}$) possibly proceeding via eq 5.

$$2\text{TDAE(l)} + 6\text{SO}_2(\text{l}) \rightarrow (\text{TDAE})(\text{O}_3\text{SSSSO}_3)(\text{s}) + \frac{1}{2}(\text{TDAE})(\text{O}_3\text{SOSO}_3)(\text{s}) + \frac{1}{2}(\text{TDAE})(\text{O}_3\text{SSO}_2)(\text{s}) \quad (5)$$

Presumably the first step in the reaction is formation of $[SO_2]_n^{2-}$ anion (we have evidence for n = 3)[9b] followed by various disproportionation reactions and further reactions with SO_2, leading to the observed products.

2.2. Characterization of 1 by Vibrational Spectroscopy and Raman Spectrum of $[TDAE]^{2+}$. IR and Raman spectra of **1** are included in Figure 1, and frequencies and intensities of bands attributed to $[O_2SSO_2]^{2-}$ are included in Table 1. The IR spectrum of $[TDAE]^{2+}$ has been reported previously, and the shift of C–N vibrations of the central N_2C–CN_2 fragment from 1340 cm^{-1} in TDAE to 1670 cm^{-1} in $[TDAE]^{2+}$ has been shown to be diagnostic for the +2 oxidation state of the dication.[15] IR bands attributed to

Scheme 2. Overall Reaction of TDAE + $2SO_2$ in Acetonitrile

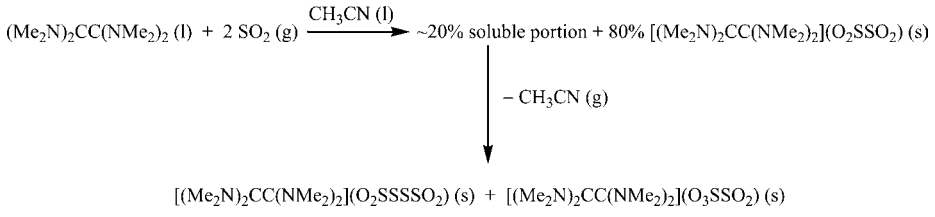

dx.doi.org/10.1021/ic4022195 | Inorg. Chem. 2013, 52, 13651–13662

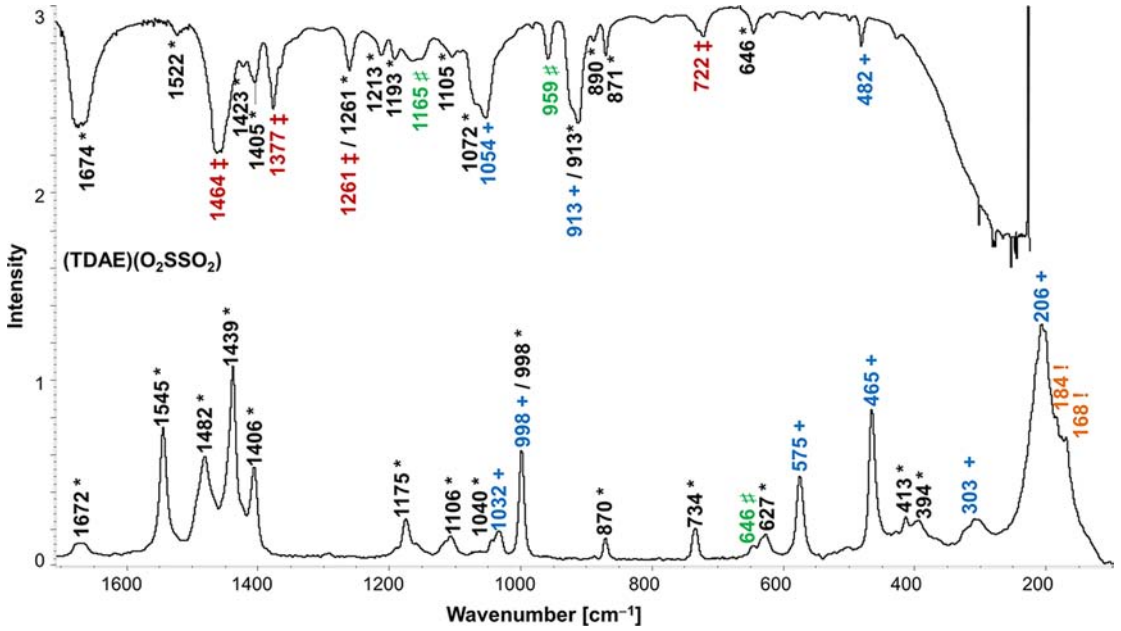

Figure 1. IR (above) and Raman (below) (10 000 scans; 0.205 W laser power) spectra of **1** from 150 to 1675 cm^{-1}: $[TDAE]^{2+}$ (black, *), $[O_2SSO_2]^{2-}$ (blue, +), band splitting (orange, !), $[O_3SSO_2]^{2-}$ (green, #), Nujol (red, ‡). Full spectra are given in the Supporting Information, Figure S15.

Table 1. Comparison and Assignments of Experimental IR and Raman Frequencies $[cm^{-1}]$ of $[O_2SSO_2]^{2-}$ in 1 and $(Et_4N)_2(O_2SSO_2)$ with [B3PW91/6-311+G(3df)] Calculated C_{2h}-Symmetric $[O_2SSO_2]^{2-}$ (relative intensities in brackets)

$(TDAE)(O_2SSO_2)$		$(Et_4N)_2(O_2SSO_2)$[14,a]		calcd C_{2h}[b] $[O_2SSO_2]^{2-}$		
IR	Raman	IR	Raman	IR	Raman	assignments[b]
1054(21)		1054(10)		1095(76)		A_u $\nu_{asym}SO_2$(ip)
	1032(4)		1041sh(2)		1068(29)	B_g $\nu_{asym}SO_2$(op)
	998(11)[c]		993(7)		1015(64)	A_g $\nu_{sym}SO_2$(ip)
913(17)		911(40)		946(100)		B_u $\nu_{sym}SO_2$(op)
	575(12)		572(9)		554(59)	A_g δOSO(ip)/νSS/δSSO
482(1)				481(3)		B_u δOSO(op)
	465(22)		463(8)		455(61)	A_g νSS/δSSO/δOSO(ip)
	303(10)		291(3)		258(24)	B_g δSSO
				216(4)		B_u δSSO
	206(100)		204(100)		150(100)	A_g νSS
	184(10)			132(<1)		A_u δSSO
	168(6)			11(<1)		A_u ρSO_2

[a]The spectrum was similar to that reported in ref 13, apart from a band at 575 cm^{-1} that was not observable in our spectrum. [b]Intensities were calculated at the B3PW91/6-311G(2d) level. Vibrations were assigned visually using the ChemCraft program:[21] ip, in phase; op, out of phase; ν, stretch; δ, bend; ρ, twist, wagging, rocking. [c]Intensity includes a vibration mode of $[TDAE]^{2+}$ (see Table 2 and Figure 2).

$[TDAE]^{2+}$ in **1** are similar to those previously published[15] and to those measured for $(TDAE)(Br_3)_2$ (Supporting Information, Table S2). However, information on the Raman spectrum of $[TDAE]^{2+}$ in the literature is scant.[19] To obtain more information on the Raman of $[TDAE]^{2+}$ we prepared $(TDAE)(Br)_2{\cdot}2H_2O$ and $(TDAE)(Br_3)_2$ and obtained their Raman spectra and X-ray structures (Supporting Information, Sections S2.1 and S2.2, respectively). The X-ray structure of $(TDAE)(Br_3)_2$ contains two crystallographically different $[TDAE]^{2+}$ (Supporting Information, Section S2.2.3) and therefore shows a slightly more complex Raman spectrum (Supporting Information, Section S2.2.2) for $[TDAE]^{2+}$ than that in $(TDAE)(Br)_2{\cdot}2H_2O$ (Supporting Information, Section S2.1.1). Otherwise, X-ray structures found for $[TDAE]^{2+}$ in $(TDAE)(Br)_2{\cdot}2H_2O$ and $(TDAE)(Br_3)_2$ and the other $[TDAE]^{2+}$-containing salts encountered in this work were similar to one another (Supporting Information Table S1) and to those previously published.[20]

Using information from other $[TDAE]^{2+}$ salts we were able to establish which bands in the Raman spectrum of **1** were attributable to $[TDAE]^{2+}$ (Table 2) and which to the anion (Table 1). Furthermore, information on $[TDAE]^{2+}$ Raman was used to identify the cation bands and assign the Raman spectra of $(TDAE)(O_3SSO_2)$, $(TDAE)(O_3SSSSO_3){\cdot}2SO_2$, and $(TDAE)(O_3SOSO_3){\cdot}SO_2$, which were prepared in the course of this work (Supporting Information, Figures S20, S21, and S22, respectively). Bands attributed to $[TDAE]^{2+}$, which are very similar to those in $(TDAE)(Br)_2{\cdot}2H_2O$ and **1**, are compared in the Supporting Information, Table S3.

The vibrational spectrum of $[O_2SSO_2]^{2-}$ in $(TDAE)(O_2SSO_2)(s)$ is in agreement with that reported for $(NEt_4)_2(O_2SSO_2)(s)$[9b,14] and that calculated for C_{2h} centro-

dx.doi.org/10.1021/ic4022195 | Inorg. Chem. 2013, 52, 13651−13662

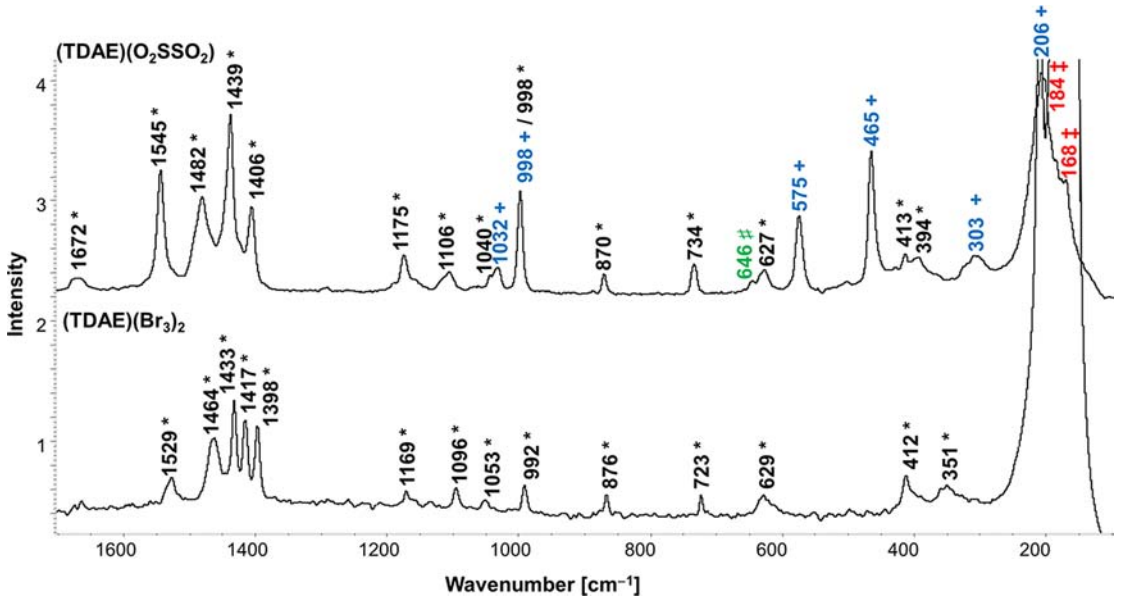

Figure 2. Comparison of the Raman spectra of **1** (above) (10 000 scans; 0.205 W laser power) and $(TDAE)(Br_3)_2$ (below) (1408 scans; 0.205 W laser power) in the 100−1700 cm^{-1} region: $[TDAE]^{2+}$ (black, *), $[O_2SSO_2]^{2-}$ (blue, +), band splitting (red, ‡), $[O_3SSO_2]^{2-}$ (green, #). For discussion and full spectra see the Supporting Information, Sections S2.2.1 and S2.2.2, and Figure S16.

symmetric $[O_2SSO_2]^{2-}$ (Figure 1, Table 1). Of the 12 expected vibrations for C_{2h} $[O_2SSO_2]^{2-}$ 9 are observed. The remaining three IR vibrations predicted to be at 216, 132, and 11 cm^{-1} are too low in frequency to be detected. Bands observed in the Raman are absent in the IR and vice versa, which is consistent with C_{2h} $[O_2SSO_2]^{2-}$ geometry (Table 1).[10,22]

There is reasonably good agreement between the observed and the calculated [B3PW91/6-311+G(3df)] $[O_2SSO_2]^{2-}$ frequencies (see Table 1). Calculated intensities are in qualitative agreement with the experimental ones, although the Raman S−O stretching modes are calculated to be more intense than those observed as reported for related species[23] and $[O_3SSSSO_3]^{2-}$ in $(TDAE)(O_3SSSSO_3)$, see Supporting Information, Section S2.6.2. The good agreement of vibrational frequencies makes it reasonable to assume that the structure of $[O_2SSO_2]^{2-}$ in **1** resembles the [B3PW91/6-311+G(3df)]-calculated C_{2h} structure shown in Figure 3. The structure of $[O_2SSO_2]^{2-}$ can be envisaged as being formed by interactions of the unpaired electrons in two $[SO_2]^{\bullet-}$ π^* orbitals (Figure 4).[24]

2.3. X-ray Crystal Structure of (TDAE)(S_4O_4)(s) (2) Containing the New Sulfur Oxyanion $[O_2SSSSO_2]^{2-}$. The structure of **2** consists of $[TDAE]^{2+}$ and $[O_2SSSSO_2]^{2-}$ ions shown in Figure 5. To a first approximation the ions crystallize in a distorted cubic lattice with 8:8 coordination of ions resulting in a CsCl-like structure (Supporting Information, Figure S24). Six of these cations are interacting with weak S···H and O···H hydrogen-bonding interactions to the neighboring anions (Supporting Information, Figure S25 and Table S7). It is not surprising that there are O···H interactions, and the S···H contacts are consistent with the calculated negative charges on the central S2 and S3 atoms (Figure 7). The structure of $[TDAE]^{2+}$ is similar to those found in other crystal structures determined in this work (Supporting Information Table S1) and reported by others in previous studies.[20]

The $[O_2SSSSO_2]^{2-}$ dianion is the first example of a new class of oxyanions, the polythionites,[26] $[O_2S(S)_nSO_2]^{2-}$ with $n \geq 1$. One of the SO_2 groups in the dianion is substantially disordered, and therefore, only data for the ordered S3S2S1O1O2 portion of the anion (Figure 5) will be referred to in subsequent discussions. The ordered geometry of O1−S1−O2 may in part arise from two long interanionic S1···S2 interactions of 3.521(1) Å [cf. S−S (S_8) = 2.055(2) Å[4] and twice the van der Waals radii of sulfur = 3.60 Å][27] linking the dianions into a centrosymmetric dimer, shown in Figure 6. These interactions are likely mostly electrostatic, with S1 (calculated charge +1.40) and S2 (calculated charge −0.36) having opposite charges. On the other hand, the S3···O2 interaction [3.325(2) Å], which is comparable to the sum of oxygen and sulfur van der Waals radii (3.32 Å),[27] is most likely not bonding since both S3 and O2 have negative charges and O2 does not lie in the same plane as the S3, S2, and S1 atoms [∠S3S2S1O2 dihedral angle 48.6(1)°]. The S3−S2 bond length of 2.003(1) Å is similar to that in S_2^- [2.005(15) Å][28] with a formal bond order of 1.5.

The SO_2 units are attached to the central S_2 fragment with longer S−S bonds of 2.254(3) and 2.337(1) Å that are similar to the S−S distance (2.389 Å) in $[O_2SSO_2]^{2-}$ of $Na_2(O_2SSO_2)$.[3] S−O distances [1.461(3) and 1.468(2) Å] are slightly less than those in $[O_2SSO_2]^{2-}$ [1.488(9)−1.523(7) Å][3,7] but longer than those in $SO_2(g)$ [1.4308(2) Å][29] (Table 3). Similarly, the OSO angle in $[O_2SSSSO_2]^{2-}$ [111.2(1)°] is greater than those in $[O_2SSO_2]^{2-}$ [108.11(4)−110.37(17)°][3,7] but less than that in $SO_2(g)$ [119.19(2)°].[29,30] The SSS angles [99.85(4)° and 99.69(9)°] and SSSS dihedral angle [87.4(1)°] are similar to those in related S_4 chains (Supporting Information, Table S8).

Electrostatic interactions between partial positive charges of hydrogen atoms and negative charges of oxygen (calculated charges O1 −1.03 and O2 −1.01), S2 (−0.36), and S3 (−0.36) atoms result in interionic contacts with distances less than the sum of the corresponding van der Waals radii (S 1.80 Å, H 1.20 Å, O 1.52 Å) (Supporting Information, Figure S25 and Table S7).[27]

2.4. Geometry, Electronic Structure, and Bonding in $[O_2SSSSO_2]^{2-}$. The observed sulfur−sulfur bond alternation in

dx.doi.org/10.1021/ic4022195 | Inorg. Chem. 2013, 52, 13651−13662

Table 2. Comparison and Assignments of Experimental IR and Raman Frequencies [cm^{-1}] of $[TDAE]^{2+}$ in 1 and $(TDAE)(Br_3)_2$ (relative intensities in brackets)

$(TDAE)(O_2SSO_2)$[a]		$(TDAE)(Br_3)_2$[b]		
IR	Raman	IR	Raman	assignments[c]
	2999 (28)		3018(7)	$\nu(CH_3)$
2984(20)	2977(38)	2984(60)	2985(9)	
	2945(39)		2943(20)	
2923(100)	2913(45)	2923(82)	2855(1)	
2853(42)	2830(11)	2853(100)	2817(1)	
			2786(<1)	
	1946(1)			?
1674(26)	1672(4)	1662(52)	1665(1)	$\nu(CN)/\nu(CC)$
	1545(20)		1529(3)	
1522(2)[d]	1482(26)		1464(6)	$\delta(CH_3)$
1423(28)	1439(32)	1456(50)	1433(5)	
1405(7)	1406(13)	1413(10)	1417(4)	$\nu(CC)/\nu(CN)$
			1398(4)	$\delta(CH_3)$
1261(8)		1205(15)		$\delta(NCN)$
1213(3), 1193(4)		1170(15)		$\rho(CH_3)/\nu(CC)$
	1175(5)		1169(2)	
1105(3)	1106(4)	1098(14)	1096(1)	combin. (CH_3)
1072(9)		1061(1)		
913(20)	1040(2)	1052(18)	1053(1)	
	998(11)		992(2)	
890(1)		879(13)		$\nu(CN)/\delta(CCN)/\delta(NCN)$
871(3)	870(2)	866(18)	876(1)	
		850(18)		
	734(3)		723(1)	
646(5)	627(5)	652(20)	629(4)	
	413(5)		412(4)	$\delta(CNC)$
	394(5)		351(5)	$\delta(CNC)/\rho([TDAE]^{2+})$

[a]Raman and IR spectra of **1** are given in Figure 1 and Supporting Information Figure S15. [b]Full IR and Raman spectra of $(TDAE)(Br_3)_2$ are given in the Supporting Information, Sections S2.2.1 and S2.2.2, respectively. [c]Assignments made by comparison to the literature (refs 15 and 19) where possible and the rest by visualizing the vibrations of calculated $[TDAE]^{2+}$ [B3PW91/6-311G+(3df)] using the ChemCraft program.[21] [d]Tentatively assigned to $[TDAE]^{+}$ monocation by Pokhodnia et al.[15]

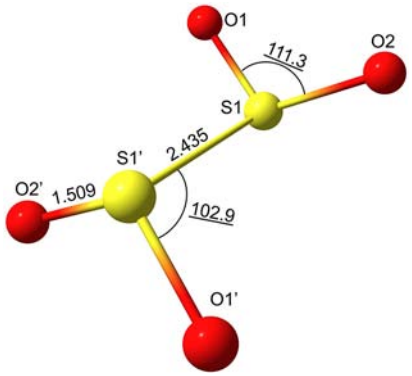

Figure 3. Calculated structure of C_{2h}-symmetric $[O_2SSO_2]^{2-}$ [B3PW91/6-311+G(3df)] with selected bond distances [Angstroms] and angles [degrees].

$[O_2SSSSO_2]^{2-}$ is reminiscent of the selenium−selenium bond alternation in the related $[I_2SeSeSeSeI_2]^{2+}$ (Figure 7) and much

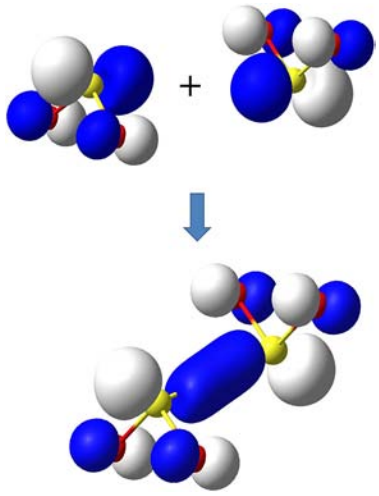

Figure 4. Unpaired electrons on SOMOs of two $[SO_2]^{\bullet-}$ bind to form $[O_2SSO_2]^{2-}$.

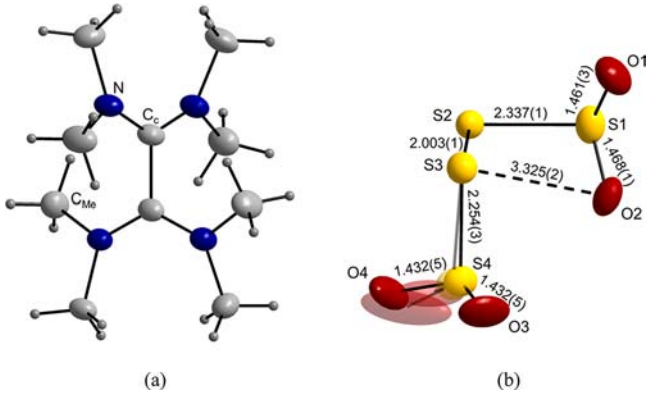

Figure 5. Diamond illustration of the (a) cation and (b) anion in the crystal structure of **2** (thermal ellipsoids drawn at the 50% probability level). Selected bond distances [Angstroms] and angles [degrees]: C_c-C_c, 1.517(3); C_c-N, 1.314(3)−1.319(3); ∠O1S1O2, 111.2(1); ∠S1S2S3S4, −87.4(1). One of the SO_2 groups is disordered (O3−S4−O4, 65%; O3A−S4A−O4A, 35% occupancy).[25] Only the major component has been labeled in the figure. Bond distances for the minor component are O4A−S4A = 1.404(7) Å, O3A−S4A = 1.412(7) Å, and S3−S4A = 2.277(6) Å.

greater than those in related S_4 chains (Supporting Information, Table S8).[32,33] We note that the related eclipsed $[I_2SeSeI_2]^{2+}$ [33,34] and isolobal $[O_2SSO_2]^{2-}$ in $Na_2(O_2SSO_2)$[3a] also have similar geometries.

In the gas-phase the optimized structure of $[O_2SSSSO_2]^{2-}$ adopts a conformation with the negatively charged oxygen atoms that are as far away from each other as possible. The energy of the experimentally observed $[O_2SSSSO_2]^{2-}$ structure is calculated to be +102.4 kJ mol^{-1} higher than the optimized minimum structure [B3PW91/6-311+G(3df)]. In the solid state the gain in overall electrostatic energy associated with hydrogen bonding, interionic contacts, and other solid-state effects is presumably enough to make the observed structure more favorable. There are nearly equal calculated negative charges on the SO_2 (−0.64) and central S_2 (−0.72) portions of the $[O_2SSSSO_2]^{2-}$ dianion. This delocalization of charge and the large S−S bond alternation (calculated and observed) implies that the overall structure in valence bond terms is

dx.doi.org/10.1021/ic4022195 | Inorg. Chem. 2013, 52, 13651−13662

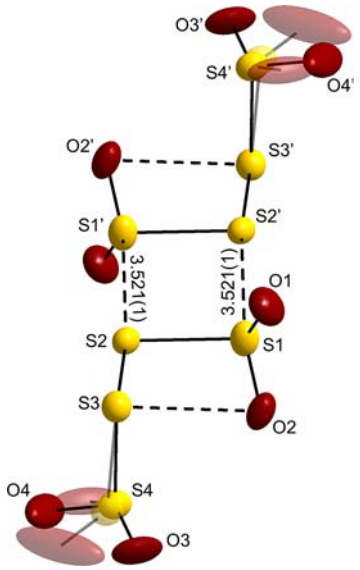

Figure 6. Diamond illustration of the interanionic $[O_2SSSSO_2]^{2-}$ S···S contacts in **2** (thermal parameters drawn at the 50% probability level).

represented by structures a, b, and b′ (Scheme 3) and other equivalent valence bond structures.

NBO analysis of $[O_2SSSSO_2]^{2-}$ suggests it has a similar all σ-bonded parent Lewis structure as that found for $[I_2SeSeSeSeI_2]^{2+}$ in a previous study (Scheme 4).[32] However, it is simpler to regard the structure of $[O_2SSSSO_2]^{2-}$ as formed from S_2 and two $[SO_2]^{\bullet-}$ where the sulfur atoms of triplet-state S_2 and $[SO_2]^{\bullet-}$ share the unpaired electrons in π^* orbitals (Figure 8) and form weak σ bonds. These S−S π^*−π^* bonds in $[O_2SSSSO_2]^{2-}$ are similar to that in $[O_2SSO_2]^{2-}$ [exp 2.389(1), calcd 2.398 Å][3,9b] and unsurprisingly longer than a conventional σ 3p−3p bond [S_8 2.055(2) Å].[4]

The much higher electron affinity of S_2 (1.670 ± 0.015 eV, 161 ± 1 kJ mol^{-1})[28] compared to that of SO_2 (exptl. 1.097 ± 0.036 eV, 106 ± 3 kJ mol^{-1} [35] and calcd 131 kJ mol^{-1}) make the resulting σ (π^*−π^*) bonds polarize toward the sulfur atoms of the S_2 unit. Effectively there is electron donation from $[SO_2]^{\bullet-}$ π^*-antibonding orbitals to S_2 π^*-antibonding orbitals which leads to an increase in the S−S bond distance of the S_2 unit in $[O_2SSSSO_2]^{2-}$ [2.003(1) Å] in comparison to S_2 (1.892 Å),[36] thereby decreasing the bond order from 2 to 1.2, giving the marked S−S bond alternation. At the same time the S−O bonds [1.461(3) and 1.468(2) Å] become shorter than those in $[SO_2]^{\bullet-}$ (Table 3, 1.50−1.52 Å). Furthermore, the atomic charges on central sulfur atoms become negative (−0.36) and atomic charges on three-coordinate sulfur atoms more positive (+1.40) compared to those in S_2 and $[SO_2]^{\bullet-}$ (+1.04), respectively. The atomic charges on oxygen atoms remain unchanged. This is because the $[SO_2]^{\bullet-}$ π^*-antibonding orbitals are mainly sulfur based as indicated by NBO analysis of $[SO_2]^{\bullet-}$ (see Supporting Information, Section S3.9) and electron donation to S_2 is effectively from the sulfur atoms of $[SO_2]^{\bullet-}$.

Stabilization of $[O_2SSSSO_2]^{2-}$ via charge delocalization compared to S_2 and $[SO_2]^{\bullet-}$ is similar to stabilization found in recently reported $[O_3SOSO_2]^{2-}$ and $[(O_2SO)_2SO_2]^{2-}$ anions.[37] In contrast to $[O_2SSSSO_2]^{2-}$, where $[SO_2]^{\bullet-}$ units donate the electrons, the SO_2 moieties of $[O_3SOSO_2]^{2-}$ and $[(O_2SO)_2SO_2]^{2-}$ function as electron acceptors that delocalize the negative charge on the $[SO_4]^{2-}$ units. The negative charges on the SO_4 moieties in $[O_3SOSO_2]^{2-}$ and $[(O_2SO)_2SO_2]^{2-}$ are lowered from −2 to −1.59 and −1.42, respectively.

2.5. Vibrational Analysis of 2. The Raman spectrum of **2** is given in Figure 9, in which the peaks attributable to $[TDAE]^{2+}$ are marked with an asterisk (*). The remaining peaks, marked with an exclamation point (!), are attributable to $[O_2SSSSO_2]^{2-}$ and show a fair agreement with the calculated Raman spectrum of the C_2-symmetric $[O_2SSSSO_2]^{2-}$ (Table 4). It is worth noting that the symmetry of the calculated $[O_2SSSSO_2]^{2-}$ structure (C_2) is higher than that found in the crystal structure (C_1), and differences between the experimental and the calculated Raman bands are to be expected. $[O_2SSSSO_2]^{2-}$ normal modes show extensive mixing of different internal coordinates. Despite the mixing, the bands at 515 and 531 cm^{-1} are associated with stretching of the central bond between the two-coordinate S atoms (S_{2c}−S_{2c}) and those at 440, 405, 280, and 218 cm^{-1} with the stretching of the bonds between two- and three-coordinate sulfur atoms (S_{2c}−S_{3c}). These frequencies are consistent with two different S−S bond lengths found in the X-ray crystal structure. The central S2−S3 bond length (Figure 5b) is much shorter than the S2−S1 bond length; thus, the S_{2c}−S_{2c} stretch is expected to be higher in frequency than the S_{2c}−S_{3c} stretch as observed. The observed frequencies for the stretching mode of the central S_{2c}−S_{2c} bond of $[O_2SSSSO_2]^{2-}$ are similar with the observed stretch for S_2^- (550 cm^{-1}),[38] consistent with the near equality of the bond length of the central S_2 unit of $[O_2SSSSO_2]^{2-}$ and S_2^- [2.005(15) Å].[28]

The S−O stretching frequencies of $[O_2SSSSO_2]^{2-}$ in **2** are higher than those in $[O_2SSO_2]^{2-}$ (Table 1) and lower than those in free SO_2(g) (ν_{asym} 1351 cm^{-1}, ν_{sym} 1147 cm^{-1})[39]

Table 3. Comparison of Experimental and Calculated [B3PW91/6-311+G(3df)] Structural Parameters of $[O_2SSO_2]^{2-}$ (X-ray) with SO_2 (ED) and $[SO_2]^{\bullet-}$(PE)[a]

	symmetry	S−S	S−O	∠O−S−O
$Na_2(O_2SSO_2)$[3]	C_{2v}	2.389(1)	1.496(2), 1.515(2)	108.11(4)
$Na_2(O_2SSO_2)\cdot 2H_2O$[7]	C_{2h}	2.298(4)	1.488(9)−1.523(7)	109.7(5), 109.2(4)
$Sn_2(O_2SSO_2)_2$[5]	C_{2v}	2.350(1)	1.503(3)−1.517(3)	110.5(3), 109.2(4)
$Zn(O_2SSO_2)\cdot Py$[6]	C_{2v}	2.386(2)	1.517(3), 1.511(3)	110.4(2)
$[O_2SSO_2]^{2-}$ (calcd)	C_{2h}	2.435	1.509	111.3
SO_2 (g, ED)[29]	C_{2v}		1.4308(2)	119.19(2)
SO_2 (calcd)	C_{2v}		1.433	119.2
$[SO_2]^{\bullet-}$ (g, PE)[31]	C_{2v}		1.52(2)	115.0(2)
$[SO_2]^{\bullet-}$ (calcd)	C_{2v}		1.508	114.5

[a]Py = pyridine; ED = electron diffraction; PE = photoelectron spectroscopy.

dx.doi.org/10.1021/ic4022195 | Inorg. Chem. 2013, 52, 13651−13662

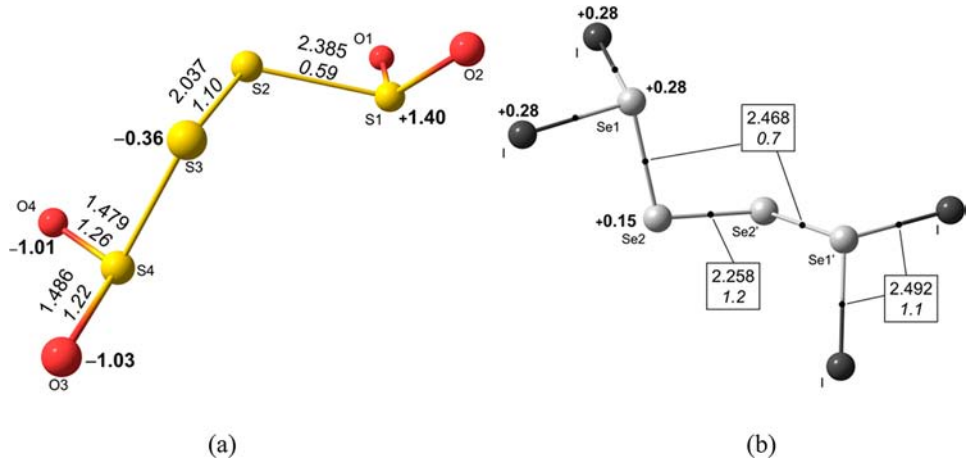

(a) (b)

Figure 7. (a) B3PW91/6-311+G(3df)-optimized structure of $[O_2SSSSO_2]^{2-}$ and (b) optimized structure of $[I_2SeSeSeSeI_2]^{2+}$ given in equilibrium $2[I_2SeSeSeSeI_2]^{2+} \leftrightarrow 2[SeI_3]^+ + [Se_6I_2]^{2+}$ in liquid SO_2 solution and unambiguously established by a combination of ^{77}Se NMR and calculations.[32] It also includes calculated natural atomic charges (bold), bond distances [Angstroms], and Wiberg Bond orders (italic).

Scheme 3. Possible Valence Bond Structures of $[O_2SSSSO_2]^{2-}$

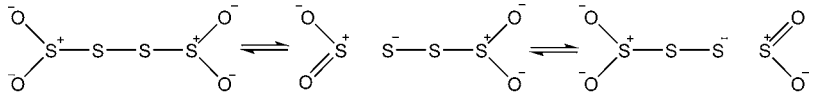

a b b'

Scheme 4. Parent Lewis Structure of $[O_2SSSSO_2]^{2-}$

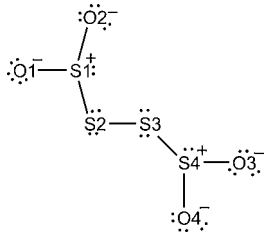

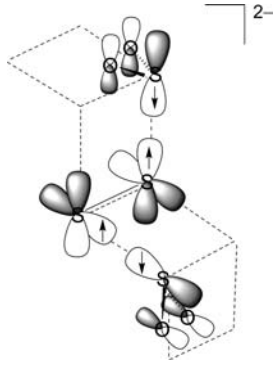

Figure 8. Bonding between S_2 and $[SO_2]^{\bullet-}$ π^* orbitals in $[O_2SSSSO_2]^{2-}$.

following the trend of the S−O bond lengths found in these anions.

2.6. Stability of $R(O_2SSSSO_2)(s)$ [R = dication] and $R'_2(O_2SSSSO_2)(s)$ [R′ = monocation] Salts toward Loss of Sulfur, and Evidence for $(TDAE)[O_2S(S)_nSO_2](s)$ (n = 1, 3). The thermodynamic stability of **2** toward losing sulfur (S_8) according to eq 6 (R = $[TDAE]^{2+}$) has been assessed using B3PW91/6-311+G(3df) calculations for gas-phase energies and VBT to estimate the lattice energy terms, Figure 10 (for details see Supporting Information, Section S3). Calculations show **2** and other salts with large molecular volumes to be stable toward losing sulfur. In contrast, $[O_2SSSSO_2]^{2-}$ salts of smaller (metal) cations (e.g., Ca^{2+}) are not stable. Furthermore, calculations suggest that stable $[O_2SSSSO_2]^{2-}$ should be accessible via large monocation salts as well according to eq 7.

$$R(O_2SSSSO_2)(s) \leftrightarrow R(O_2SSO_2)(s) + \frac{1}{4}S_8(s) \quad (6)$$

$$R_2(O_2SSSSO_2)(s) \leftrightarrow R_2(O_2SSO_2)(s) + \frac{1}{4}S_8(s) \quad (7)$$

In addition to estimating the stability of **2** toward losing sulfur, the thermodynamics of reactions of **1** with various stoichiometric amounts to S_8 to produce different salts of type $(TDAE)[O_2S(S)_nSO_2](s)$ (n = 1−4) were estimated and are shown in Table 5. Calculations show that several members of this new class of $(TDAE)[O_2S(S)_nSO_2](s)$ salts are thermodynamically accessible (calculated structures with bond distances, natural atomic charges, and Wiberg bond orders are given in Figure S27, Supporting Information). The favorable energetics suggest that it is likely that one of the steps in the reaction of TDAE and SO_2 leading to **2** (Scheme 2) is that of **1** and elemental sulfur.

Preliminary results show that **1** takes up S_8 in acetonitrile (Supporting Information, Section S2.7 and Figure S23). Raman spectra imply there are at least two sulfur oxyanions formed that are different from $[O_2SSSSO_2]^{2-}$ and other known sulfur oxydianions. Reactions of $(TDAE)(O_2SS_nSO_2)(s)$ (n = 0−3) with 1/8 $S_8(s)$ are thermodynamically favorable, but reaction with $n \geq 4$ is marginal. These findings imply that numerous new sulfur oxyanions of large countercations await discovery. It also implies that a potentially rich chemistry of $[O_2SSO_2]^{2-}$ is accessible for salts of large cations, similar to that found for $[N(CH_3)_4]_2(SO_4)(s)$, which reacts with SO_2 to give $[N(CH_3)_4]_2[(SO_4)\cdot nSO_2](s)$ (n = 1, 2).[37]

dx.doi.org/10.1021/ic4022195 | Inorg. Chem. 2013, 52, 13651−13662

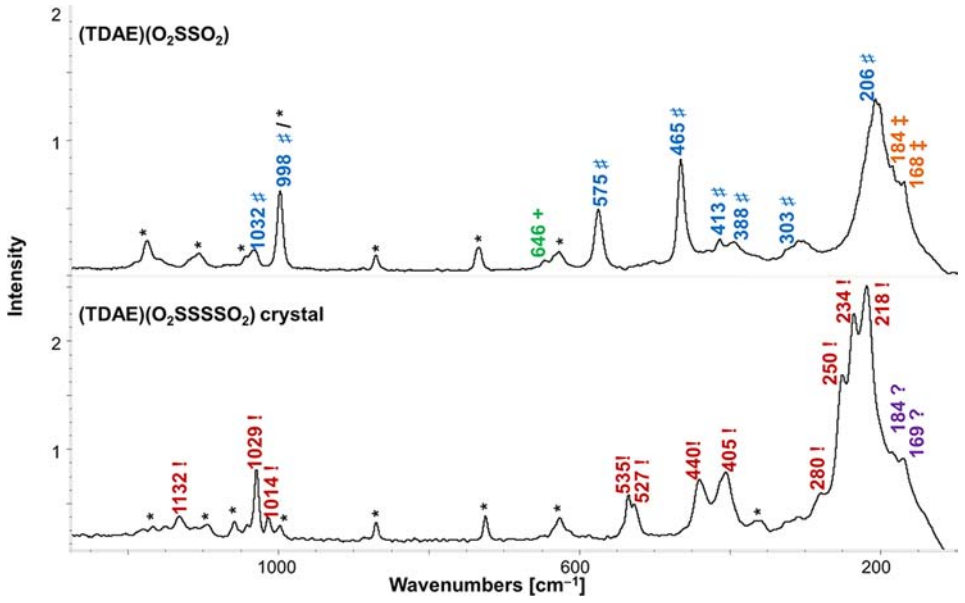

Figure 9. Comparison of the Raman spectra of **1** (above) (10000 scans; 0.205 W laser power) and crystals of **2** (below) (2048 scans; 0.157 W laser power) in 100 − 1260 cm^{-1} region. $[TDAE]^{2+}$ (black, *); $[O_2SSSSO_2]^{2-}$ (red, !), band splitting (orange, ‡); $[O_2SSO_2]^{2-}$ (blue, #); unassigned bands (purple, ?) and impurity $O_3SSO_2^{2-}$ (green, +). Full Spectra given in Figure S15, Supporting Information.

Table 4. Comparison and Assignment of Experimental Raman Frequencies [cm^{-1}] of the C_1-Symmetric $[O_2SSSSO_2]^{2-}$ in 2 with Normal Modes Calculated [B3PW91/6-311+G(3df)] for the C_2-Symmetric $[O_2SSSSO_2]^{2-}$ Structure (relative intensities in brackets)

$[O_2SSSSO_2]^{2-}$ in **2**	calcd $[O_2SSSSO_2]^{2-a}$	assignments[b]
	1173(4)	ν_{asym} SO_2 (ip)[c]
1132(7)	1172(49)	ν_{asym} SO_2 (op)[c]
1029(10)	1058(100)	ν_{sym} SO_2 (ip)[c]
1014(4)	1046(21)	ν_{sym} SO_2 (op)[c]
535(15)	531(43)	$\nu S_cS_c/\delta OSO$ (ip)
527(sh)	515(38)	$\nu S_cS_c/\delta OSO$ (ip)[d]
440(28)	432(92)	$\nu S_cS_t/\delta OSO$ (ip)/δSSO
405(33)	423(10)	$\nu S_cS_t/\delta OSO$ (op)/δSSO
280(14)		
250(40)	261(14)	$\nu S_cS_t/\delta SSO$ (ip)/$\rho[S_4O_4]^{2-}$
234(53)	237(5)	δS_cS_tO (op)
218(100)	189(22)	νS_cS_t
184(sh) + 169(sh) (57)	171(47)	$\nu S_cS_t/\rho[S_4O_4]^{2-}$

[a]Calculated Raman spectrum of C_2-symmetric $[O_2SSSSO_2]^{2-}$ [B3PW91/6-311+G(3df)] shows 18 Raman-active vibrations. However, the calculated vibrations at 517(<1), 91(4), 83(32), 40(1), and 32(2) cm^{-1} are too low in intensity or too low in frequency to be observed in the experimental spectrum. [b]Assigned by visualizing the vibrations using the ChemCraft program:[21] ip, in phase; op, out of phase; ν, stretch; δ, bend; ρ, twist, wagging, or rocking. [c]ip or op vibrations of the same SO_2 relative to the second SO_2 in $[O_2SSSSO_2]^{2-}$. [d]νSS (op) relative to δOSO

3. CONCLUSIONS

We predicted the thermodynamics of the reaction of organic liquid TDAE with gaseous SO_2 to give tetrakis(dimethylamino)ethane-1,2-bis(ylium) dithionite (**1**) to be favorable and subsequently prepared analytically pure insoluble purple **1** in a simple one-step redox reaction in 80% yield. Preliminary TDDFT calculations suggested that the purple color could be related to a charge-transfer transition from a dithionite-centered orbital to a low-lying $[TDAE]^{2+}$ orbital. Our approach illustrates the utility of predictive thermodynamics, estimating lattice energies by the VBT method and gas-phase terms by DFT calculations and implies that other related organic reducing agents could be used similarly, producing a family of high-purity dithionite salts of large organic cations. The IR spectrum of $[TDAE]^{2+}$ has been well characterized, but there was a paucity of information on the Raman. To establish the Raman spectrum of $[TDAE]^{2+}$ we prepared TDAE(A) (A = $2Br^-$, $2Br^-\cdot 2H_2O$, $2[Br_3]^-$), characterized them by X-ray crystallography, and analyzed their Raman spectra. Vibrational spectroscopy and B3PW91/6-311+G(3df) calculations were used to show that $[O_2SSO_2]^{2-}$ in **1** has a C_{2h} centrosymmetric structure. In addition to **1**, reaction of SO_2 and TDAE produced soluble product out of which orange crystals were obtained. X-ray crystallography showed the crystals to be **2** containing $[O_2SSSSO_2]^{2-}$, the first member of a new class of oxyanions of sulfur, the polythionites, cf. the long known polythionates.[2b] The structure of $[O_2SSSSO_2]^{2-}$ contains a sulfur chain with a marked S−S bond alternation unlike other tetrasulfur chains that exhibit similar S−S bond lengths. Gas-phase calculations [B3PW91/6-311+G(3df)] show that the negative charge of $[O_2SSSSO_2]^{2-}$ is almost equally shared between the two terminal SO_2 groups and the central SS fragment. The bonding between these fragments arises from interaction of the unpaired electrons in the SOMO π^*-antibonding orbitals of the two $[SO_2]^{\bullet-}$ with two unpaired electrons in the mutually perpendicular SOMO π^*-antibonding orbitals of the triplet-state diradical S_2 (Figure 8). Thermodynamic stability of **2** toward losing sulfur and giving **1** was estimated, and **2** was found to be stable. However, if $[TDAE]^{2+}$ in **2** is replaced by a smaller cation, e.g., Ca^{2+}, then the corresponding salt is not stable anymore. Thus, the chemistry and stability of oxyanions of sulfur are shown to be dependent on countercation size. This and preliminary experimental observations imply that numerous hitherto unknown oxyanions of sulfur can be prepared as salts of suitably large countercations. It is possible that with larger dications than $[TDAE]^{2+}$

dx.doi.org/10.1021/ic4022195 | Inorg. Chem. 2013, 52, 13651−13662

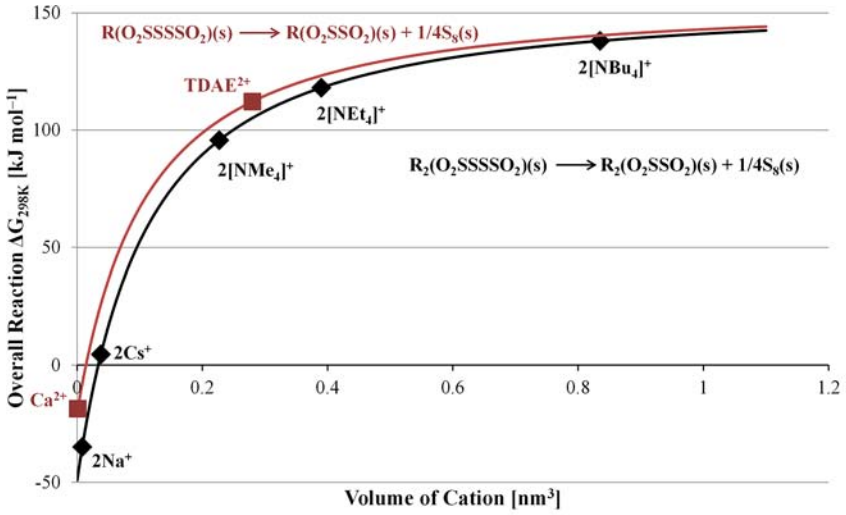

Figure 10. Stability of $R[O_2SSSSO_2](s)$ and $R_2[O_2SSSSO_2](s)$ with respect to loss of sulfur according to reactions 6 and 7, respectively, as a function of cation volume (For calculation details see Supporting Information, Section S3.7).

Table 5. Calculated Enthalpies[a] and Gibbs Free Energies of Reaction [kJ mol^{-1}] for $(TDAE)(O_2SSO_2)(s) + 1/8S_8(s) \leftrightarrow (TDAE)(O_2SS_nSO_2)(s)$

	ΔH	ΔG(298 K)
$(TDAE)(O_2SSO_2)(s) + 1/8S_8(s) \leftrightarrow (TDAE)(O_2SSSO_2)(s)$	−60	−44
$(TDAE)(O_2SSSO_2)(s) + 1/8S_8(s) \leftrightarrow (TDAE)(O_2SSSSO_2)(s)$	−65	−66
$(TDAE)(O_2SSSSO_2)(s) + 1/8S_8(s) \leftrightarrow (TDAE)(O_2SSSSSO_2)(s)$	−25	−21
$(TDAE)(O_2SSSSSO_2)(s) + 1/8_8(s) \leftrightarrow (TDAE)(O_2SSSSSSO_2)(s)$	−5	+6

[a]Calculation details given in Supporting Information Section S3.8.

salts of $[SO_2]^-$ rather than $[O_2SSO_2]^{2-}$ may be accessible (see Supporting Information Section S3.5).

The results of this report are in stark contrast to the fact that apart from recent characterizations of tetrasulfate anion $[(SO_4)(SO_3)_3]^{2-}$ [40] and $[(SO_4)(SO_2)_x]^{2-}$ (x = 1, 2) anions[37] almost all of the known sulfur oxyanions have been identified or discovered prior to the end of the 19th century.[2b] We have shown here and elsewhere that with the use of sufficiently large countercations the chemistry of sulfur oxyanions can be vastly extended.

The origin of the purple color of $(TDAE)(O_2SSO_2)(s)$ and its reaction with elemental sulfur warrant further investigation.

4. EXPERIMENTAL SECTION

4.1. General Procedures. The reaction vessel used was a two-tube Pyrex H vessel equipped with two Rotaflo Teflon in glass valves and a medium sintered glass frit (Supporting Information, Figure S1).[12] FT-IR spectra were recorded on a Thermo Nicolet NEXUS 470 FT-IR, with 2 cm^{-1} resolution and 32 scans unless otherwise specified. Samples were quickly prepared and taken as Nujol mulls between KBr plates that were wrapped on the outer edges with Teflon tape. FT-Raman spectra were recorded on a Thermo Nicolet 6700 FT-IR equipped with a Thermo Nicolet NXR FT-Raman accessory at 298 K using a Nd:YVO_4 laser (emission wavelength 1064 nm; detector Ge; resolution 4 cm^{-1}; 180° excitation unless otherwise specified) with the compounds sealed in melting point tubes. Intensities of the bands were found by the area under the curve calculated by the OMNIC program[41] and fitted to 100. Elemental analyses were carried out by Galbraith Laboratories, Inc., Knoxville, TN.

4.2. X-ray Crystallography. Single crystals were coated with Paratone-N oil, mounted using a polyimide MicroMount, and frozen in the cold nitrogen stream of the goniometer. A hemisphere of data was collected on a Bruker AXS P4/SMART 1000 diffractometer[42] using ω and θ scans with a scan width of 0.3° and 20 s exposure times [10 s for the structure of $(TDAE)(O_2SSSSO_2)$]. Detector distance was 5 cm. Data were reduced (SAINT)[43] and corrected for absorption (SADABS).[44] Structures were solved by direct methods and refined by full-matrix least-squares on F^2 (SHELXTL).[45] All non-hydrogen atoms were refined using anisotropic displacement parameters. Water hydrogen atoms were found in Fourier difference maps and refined using bond distance and angle restraints. Remaining hydrogen atoms were included in calculated positions and refined using a riding model. A summary of the data collection parameters is provided in Table 6. The Diamond 3.2 program[46] was used for graphics.

4.3. Materials. Sulfur dioxide (SO_2, Liquid Air, 99.999%) was vacuum distilled to 4 Å molecular sieves in a 500 mL round-bottom flask (rbf) equipped with a Whitey (1KS4) valve, stored for 24 h, then distilled onto CaH_2 in a 500 mL rbf equipped with a Whitey (1KS4) valve, and stored for at least 24 h before use. $(Me_2N)_2C{=}C(NMe_2)_2$ (TDAE) was purchased from Oakwood Products, Inc. (technical purity), stored in the drybox at −20 °C, and used as received. Bromine (Fisher Scientific) was stored over CaH_2 before use. Anhydrous acetonitrile from Caledon Biotech Reagent was dried over fresh CaH_2 and degassed. Diethyl ether was obtained from the solvent purification system at the chemistry department of UNB and stored over Na in the drybox.

4.4. Quantum Chemical Calculations. All calculations were carried out with the Gaussian 09 program package.[47] B3PW91 functional[48] with the 6-311+G(3df)[49] basis set was employed for geometry optimizations and frequency calculations. NBO analyses[50] were performed using NBO 3.1 as implemented in the Gaussian 09 package.

4.5. Preparation of $(TDAE)(O_2SSO_2)(s)$ (1) and $(TDAE)$-$(O_2SSSSO_2)(s)$ (2). TDAE (1.0294 g, 5.139 mmol) was added to the left-hand side of a flame-dried H vessel (see Supporting Information, Figure S1) and degassed 3 times. Acetonitrile (15.7484g) was condensed to TDAE, resulting in a yellow solution that was degassed, and 0.6227g (9.720 mmol, 1.892 mol equiv) of SO_2

dx.doi.org/10.1021/ic4022195 | Inorg. Chem. 2013, 52, 13651−13662

Table 6. Crystal Data and Refinement Parameters of (TDAE)(A) (A = $[O_2SSSSO_2]^{2-}$, 2$[Br]^-$·2H_2O, 2$[Br_3]^-$)

	(TDAE)(O_2SSSSO_2)	(TDAE)$(Br)_2$·2H_2O	(TDAE)$(Br_3)_2$
formula	$C_{10}H_{24}N_4O_4S_4$	$C_{10}H_{28}Br_2N_4O_2$	$C_{10}H_{24}Br_6N_4$
fw	392.57	396.18	679.79
T [K]	188(1)	173(1)	173(2)
cryst size [mm]	0.20, 0.20, 0.20	0.40, 0.40, 0.05	0.40, 0.30, 0.20
color, habit	orange, parallelepiped	colorless, plate	yellow, rod
space group	$P2_1/c$	$Pbca$	$P2/n$
a [Å]	8.8871(10)	9.2274(12)	16.186(4)
b [Å]	12.3534(14)	14.670(2)	8.1664(18)
c [Å]	16.1822(18)	25.607(4)	16.298(4)
β [deg]	91.517(2)	90	104.059(4)
V [Å^3]	1776.0(3)	3466.3(8)	2089.8(8)
Z	4	8	4
density [g cm^{-3}]	1.468	1.518	2.161
no. of collected reflns	12 086	22 577	29 325
no. of independent reflns	3973	3926	9199
R_1/wR_2 [$I > 2(I)$]	0.0476, 0.1230	0.0331, 0.0845	0.0452, 0.1169
residual electron density/e Å^{-3}	0.8970	−0.647 and 0.942	−0.920 and 1.395

was added. The solid orange reaction mixture became dark red on warming. Immediately a purple solid precipitated under an orange solution. The reaction vessel was placed in the drybox antechamber which was filled with dry N_2 in order to minimize moisture diffusion into the vessel and to rigorously exclude light. After 12 h the IR spectra of the gas-phase over the reaction mixture showed the absence of SO_2. The reddish orange solution was carefully filtered to the right-hand side of the H vessel, without further excluding of light. The purple precipitate was washed four times by back condensing the solvent from the filtrate and dried under vacuum to yield 1.280 g of the purple product in 80% isolated yield according to eq 3. The reddish orange filtrate was left to crystallize in a vial in the drybox. Reddish orange crystals of **2** grew from the filtrate, and a pale yellow powder settled at the bottom of the vial after a period of several weeks. The yellow powder was confirmed to be the pyrosulfite salt (TDAE)(O_3SSO_2) by vibrational analysis (see Supporting Information, Section S2.6.1). Anal. Calcd for the purple dithionite salt $C_{10}H_{24}N_4S_2O_4$: C, 36.57; H, 7.37; N, 17.06; S, 19.52. Found: C, 36.46; H, 7.21; N, 16.58; S, 19.38.

4.6. Reaction of Liquid TDAE with Excess of Liquid SO_2. TDAE (0.140 g, 0.699 mmol) was measured to an H vessel (Supporting Information, Figure S1), degassed twice, and added to 4.173 g (65.132 mmol, 93 mol equiv) of SO_2 on the other side of the H vessel, at temperatures between −176 and 0 °C. The solution that was formed turned immediately red with concurrent formation of an orange precipitate. At room temperature the solution separated into two phases, the upper having orange color and the lower red color. After several months two different types of colorless crystals were observed. The solution was filtered and evaporated, resulting in a slightly yellow solid. The first type of colorless crystals was shown by Raman spectroscopy and X-ray crystallography to be (TDAE)-(O_3SSSSO_3)·2SO_2[51] with one disordered SO_2, and the second type of crystals was likely (TDAE)(O_3SOSO_3)·SO_2, although, the anion was highly disordered.[52] The Raman spectrum of the slightly yellow solid was consistent with the presence of (TDAE)(O_3SSSSO_3), (TDAE)(O_3SOSO_3), and (TDAE)(O_3SSO_2). Thus, reactions of TDAE with liquid SO_2 led to (TDAE)(O_3SSSSO_3) (preliminary X-ray,[51] Raman analysis see Supporting Information, Section S2.6.2), (TDAE)(O_3SOSO_3) (preliminary X-ray,[52] Raman analysis see Section S2.6.3, Supporting Information), and some (TDAE)(O_3SSO_2) (Raman analysis see Section S2.6.1, Supporting Information), possibly proceeding via eq 5.

4.7. Preparation of (TDAE)$(Br)_2$·2H_2O and (TDAE)$(Br_3)_2$. (TDAE)$(Br)_2$ and (TDAE)$(Br_3)_2$ were prepared by reacting an ether solution of TDAE with 1 and 3 mol equiv of bromine, respectively (eq 8, for details see Supporting Information, Sections S2.1 and S2.2). Crystals of (TDAE)$(Br)_2$·2H_2O were obtained from a solution of (TDAE)$(Br)_2$ dissolved in water; (TDAE)$(Br_3)_2$ crystals were obtained from an acetonitrile solution. Bromide salts were characterized by X-ray crystallography (Supporting Information, Sections S2.1.2 and S2.2.3) and vibrational spectroscopy (Sections S2.1.1, S2.2.1, and S2.2.2, Supporting Information). The crystal structure of (TDAE)$(Br_3)_2$ showed two different $[Br_3]^-$ anions, one asymmetric and the other nearly centrosymmetric. In the Raman spectrum of (TDAE)$(Br_3)_2$ the $[Br_3]^-$ vibration at 181 cm^{-1} is assigned to the symmetric stretch of the almost symmetric $[Br_3]^-$ [Br−Br 2.504(1) and 2.588(1) Å]. Bands at 160 and 208 cm^{-1} are assigned to the stretches of the longer [2.611(1) Å] and shorter [2.482(2) Å] Br−Br bonds of the asymmetric $[Br_3]^-$.

$$\mathrm{TDAE(l)} + n\mathrm{Br_2} \xrightleftharpoons{\mathrm{Et_2O}} (\mathrm{TDAE^{2+}})(\mathrm{Br}_n^-)_2 \ (n = 1, 3) \qquad (8)$$

■ ASSOCIATED CONTENT

Supporting Information

Details of thermodynamic and TDDFT calculations, comparison spectra and tables with assignments for vibrational spectroscopy, crystal packing figures for **2**, experimental details of the syntheses, spectroscopic characterizations, and X-ray analyses of (TDAE)$(Br)_2$·2H_2O and (TDAE)$(Br_3)_2$, details of the reaction of TDAE with excess of SO_2, vibrational characterization of the resulting products, details of the reaction of **1** with S_8, and vibrational analysis of TDAE(A) (A = $[O_3SSSSO_3]^{2-}$, $[O_3SOSO_3]^{2-}$, and $[O_3SSO_2]^{2-}$). CCDC 832205, CCDC 832203, and CCDC 832204 contain supplementary crystallographic data for this paper. This material is available free of charge via the Internet at http://pubs.acs.org.

■ AUTHOR INFORMATION

Corresponding Author

*E-mail: passmore@unb.ca.

Notes

The authors declare no competing financial interest.

■ ACKNOWLEDGMENTS

We thank the Natural Sciences and Engineering Research Council (NSERC) of Canada and Academy of Finland (J.M.R.) for funding. ACEnet, the regional high-performance computing consortium for universities in Atlantic Canada, and CSC-IT Center for Science Ltd. in Finland are acknowledged for providing computational resources.

■ REFERENCES

(1) (a) Greenwood, N. N.; Earnshaw, A. *Chemistry of the Elements*, 2nd ed.; Pergamon Press: Oxford, U.K., 1997; p 720. (b) Louis-Andre, O.; Gelbard, G. *Tetrahedron Lett.* **1985**, *26*, 831. (c) Sayre, L.; Jensen, F. R. *J. Org. Chem.* **1979**, *44*, 228. (d) Scaife, C. W. J.; Wilkins, R. G. *Inorg. Chem.* **1980**, *19*, 3244.

(2) (a) Berzelius, J. J. *Lehrbuch der Chemie*; Arnold: Dresden, Germany, 1825; p 472. (b) Mellor, J. W. A. *Comprehensive Treatise on Inorganic and Theoretical Chemistry*; Longmans, Green and Co., LTD: London, U.K., 1940; Vol. *10*.

(3) (a) Dunitz, J. D. *Acta Crystallogr.* **1956**, *9*, 579. (b) Meyer, B. *Chem. Rev.* **1976**, *76*, 367.

(4) Rettig, S. J.; Trotter, J. *Acta Crystallogr.* **1987**, *C43*, 2260.

(5) Magnusson, A.; Johansson, L. G. *Acta Chem. Scand.* **1982**, *A36*, 429.

(6) Kiers, C. T.; Vos, A. *Acta Crystallogr.* **1978**, *B34*, 1499.
(7) Weinrach, J. B.; Meyer, D. R.; Guy, J. T.; Michalski, P. E., Jr.; Carter, K. L.; Grubisha, D. S.; Bennett, D. W. *J. Crystallogr. Spectrosc. Res.* **1992**, *22*, 291.
(8) Steudel, R.; Steiger, T. *J. Mol. Structure (THEOCHEM)* **1993**, *284*, 55.
(9) (a) Pandey, R. A.; Biswas, R.; Chakrabarti, T.; Devotta, S. *Crit. Rev. Environ. Sci. Technol.* **2005**, *35*, 571. (b) Bruna, P.; Greer, S.; Grein, F.; Paulose, T. A. P.; Passmore, J.; Rautiainen, J. M.; Schriver, M. J. Manuscript in preparation.
(10) Lough, S. M.; McDonald, J. W. *Inorg. Chem.* **1987**, *26*, 2024.
(11) Mincey, T.; Traylor, T. G. *Bioinorg. Chem.* **1978**, *9*, 409.
(12) Bruna, P. J.; Greer, S.; Passmore, J.; Rautiainen, J. M. *Inorg. Chem.* **2011**, *50*, 1491.
(13) Hodgeman, W. C.; Weinrach, J. B.; Bennett, D. W. *Inorg. Chem.* **1991**, *30*, 1611.
(14) Greer, S., M.Sc. Dissertation, University of New Brunswick, 2012.
(15) (a) Pokhodnia, K. I.; Papavassiliou, J.; Umek, P.; Omerzu, A.; Mihailovic, D. *J. Chem. Phys.* **1999**, *110*, 3606. (b) Wiberg, N. *Angew. Chem., Int. Ed. Engl.* **1968**, *7*, 766.
(16) (a) Jenkins, H. D. B.; Roobottom, H. K.; Passmore, J.; Glasser, L. *Inorg. Chem.* **1999**, *38*, 3609. (b) Jenkins, H. D. B. *J. Chem. Educ.* **2005**, *82*, 950. (c) Jenkins, H. D. B.; Glasser, L. *Inorg. Chem.* **2006**, *45*, 1754.
(17) (a) ΔG_{vap}(298 K) of TDAE has been estimated from ΔH_{vap} = 53.66 kJ mol^{-1} and a boiling point of TDAE 59 °C by assuming ideal gas behavior. (b) Anderson, D. F. *IEEE Trans. Nucl. Sci.* **1981**, *NS-28* (1), 842.
(18) Nakai, H.; Mizuno, M.; Nishioka, T.; Koga, N.; Shiomi, K.; Miyano, Y.; Irie, M.; Breedlove, B. K.; Kinoshita, I.; Hayashi, Y.; Ozawa, Y.; Yonezawa, T.; Toriumi, K.; Isobe, K. *Angew. Chem., Int. Ed.* **2006**, *45*, 6473.
(19) (a) Wiberg, N.; Buchler, J. W. *Chem. Ber.* **1963**, *96*, 3223. (b) Wiberg, N. *Angew. Chem., Int. Ed. Engl.* **1968**, *7*, 766. (c) Tanaka, K.; Sato, T.; Yamabe, T. *J. Phys. Chem.* **1996**, *100*, 3980.
(20) (a) Gritsan, N. P.; Lonchakov, A. V.; Lork, E.; Mews, R.; Pritchina, E. A.; Zibarev, A. V. *Eur. J. Inorg. Chem.* **2008**, 1994. (b) Tyrra, W.; Naumann, D.; Pohl, H.; Pantenburg, I. *Z. Anorg. Allg. Chem.* **2003**, *629*, 1039. (c) Kolomeitsev, A.; Médebielle, M.; Kirsch, P.; Lork, E.; Röschenthaler, G.-V. *J. Chem. Soc., Perkin Trans. I* **2000**, 2183. (d) Bock, H.; Borrmann, H.; Havlas, Z.; Oberhammer, H.; Ruppert, K.; Simon, A. *Angew. Chem., Int. Ed. Engl.* **1991**, *30*, 1678. (e) Fox, J. R.; Foxman, B. M.; Guarrera, D.; Miller, J. S.; Calabrese, J. C.; Reis, A. H., Jr. *J. Mater. Chem.* **1996**, *6*, 1627. (f) Bock, H.; Ruppert, K.; Merzweiler, K.; Fenske, D.; Goesmann, H. *Angew. Chem., Int. Ed. Engl.* **1989**, *28*, 1684.
(21) Zhurko, G. A.; Zhurko, D. A. ChemCraft 1.6; http://www.chemcraftprog.com.
(22) Takahashi, H.; Kaneko, N.; Miwa, K. *Spectrochim. Acta* **1982**, *38A*, 1147.
(23) (a) Decken, A.; Knapp, C.; Nikiforov, G. B.; Passmore, J.; Rautiainen, J. M; Wang, X.; Zeng, X. *Chem.—Eur. J.* **2009**, *15*, 6504. (b) Kumar, A.; McGrady, G. S.; Passmore, J.; Grein, F.; Decken, A. *Z. Anorg. Allg. Chem.* **2012**, *638*, 744.
(24) Wong, M. W.; Steudel, Y.; Steudel, R. *Chem.—Eur. J.* **2007**, *13*, 502 and references therein..
(25) X-ray structures of several crystals from two independent syntheses gave the same results each time. Disorder was present as well as occupancies (65% and 35%) for the two components of the disordered SO_2 unit for two complete data sets. Due to close proximity of some of the atoms, bond distances and thermal parameters could not be refined freely, which lead to relatively large thermal parameters for the minor component of the disorder model.
(26) (a) The term polythionite has appeared in previous literature where it has been in our view used inaccurately to refer to chemically reduced SO_2 species of type $Li(SO_2)_n$. In this contribution we use the polythionite term to refer to oxyanions with $[O_2S(S)_nSO_2]^{2-}$ ($n \geq 1$) structures that are analogous to the series of polythionates $[O_3S(S)_nSO_3]^{2-}$. (b) Potteau, E.; Levillain, E.; Lelieur, J.-P. *New J. Chem.* **1999**, *23*, 1117. (c) Potteau, E.; Levillain, E.; Lelieur, J.-P. *J. Electroanal. Chem.* **1999**, *476*, 15.
(27) Bondi, A. *J. Phys. Chem.* **1964**, *68*, 441.
(28) Moran, S.; Ellison, G. B. *J. Phys. Chem.* **1988**, *92*, 1794.
(29) Holder, C. H.; Fink, M. *J. Chem. Phys.* **1981**, *75*, 5323.
(30) Post, B.; Schwartz, R. S.; Fankuchen, I. *Acta Crystallorg.* **1952**, *5*, 372.
(31) Nimlos, M. R.; Ellison, G. B. *J. Phys. Chem.* **1986**, *90*, 2574.
(32) (a) Carnell, M. M.; Grein, F.; Murchie, M. P.; Passmore, J.; Wong, C.-M. *J. Chem. Soc., Chem. Commun.* **1986**, 225. (b) Brownridge, S.; Calhoun, L.; Jenkins, H. D. B.; Laitinen, R. S.; Murchie, M.; Passmore, J.; Pietikäinen, J.; Rautiainen, J. M.; Sanders, J. C. P.; Schrobilgen, G. J.; Suontamo, R. J.; Tuononen, H. M.; Valkonen, J. U.; Wong, C. M. *Inorg. Chem.* **2009**, *48*, 1938.
(33) Brownridge, S.; Crawford, M. J.; Du, H.; Harcourt, R. D.; Knapp, C.; Laitinen, R. S.; Passmore, J.; Rautiainen, J. M.; Suontamo, R. J.; Valkonen, J. *Inorg. Chem.* **2007**, *46*, 681.
(34) Nandana, W. A. S.; Passmore, J.; White, P. S.; Wong, C. M. *Inorg. Chem.* **1990**, *29*, 3529.
(35) Celotta, R. J.; Benett, R. A.; Hall, J. L. *J. Chem. Phys.* **1974**, *60*, 1740.
(36) Steudel, R. *Angew. Chem.* **1975**, *87*, 683; *Angew. Chem., Int. Ed. Engl.* **1975**, *14*, 655.
(37) Bruna, P.; Decken, A.; Grein, F.; Passmore, J.; Rautiainen, J. M.; Richardson, S.; Whidden, T. *Inorg. Chem.* **2013**, *52*, 7193.
(38) Holzer, W.; Murphy, W. F.; Bernstein, H. J. *J. Mol. Spectrosc.* **1969**, *32*, 13.
(39) Maillard, D.; Allavena, M.; Perchard, J. P. *Spectrochim. Acta* **1975**, *31A*, 1523.
(40) Logemann, C.; Klüner, T.; Wickleder, M. S. *Angew. Chem., Int. Ed.* **2012**, *51*, 4997.
(41) *OMNIC 8.1*; Thermo Fisher Scientific Inc.; Mississauga, ON, 2009.
(42) *SMART 5.054*; Bruker AXS, Inc.; Madison, WI, 1999.
(43) *SAINT 7.23A*; Bruker AXS, Inc.; Madison, WI, 2006.
(44) Sheldrick, G. *SADABS*; Bruker AXS, Inc., Madison,WI, 2008.
(45) (a) Sheldrick, G. M. SHELXTL. *Acta Crystallorg.* **2008**, *A64*, 112. (b) *GEMINI 1.0*; Bruker AXS, Inc.; Madison, WI, 1999 (c) *RLATT 2.72*; Bruker AXS, Inc.; Madison, WI, 1999; (d) *CELL_NOW*, V. 2008/2; Bruker AXS, Inc.: Madison, WI, 2008. (e) Parsons, S.; Gould, R. O. *ROTAX*; Oxford University, Oxford, U.K., 2001.
(46) Brandenburg, K.; Brandt, M. *DIAMOND 3.2h*; Crystal Impact: Bonn, Germany.
(47) Frisch, M. J.; Trucks, G. W.; Schlegel, H. B.; Scuseria, G. E.; Robb, M. A.; Cheeseman, J. R.; Scalmani, G.; Barone, V.; Mennucci, B.; Petersson, G. A.; Nakatsuji, H.; Caricato, M.; Li, X.; Hratchian, H. P.; Izmaylov, A. F.; Bloino, J.; Zheng, G.; Sonnenberg, J. L.; Hada, M.; Ehara, M.; Toyota, K.; Fukuda, R.; Hasegawa, J.; Ishida, M.; Nakajima, T.; Honda, Y.; Kitao, O.; Nakai, H.; Vreven, T.; Montgomery, J. A. Jr.; Peralta, J. E.; Ogliaro, F.; Bearpark, M.; Heyd, J. J.; Brothers, E.; Kudin, K. N.; Staroverov, V. N.; Kobayashi, R.; Normand, J.; Raghavachari, K.; Rendell, A.; Burant, J. C.; Iyengar, S. S.; Tomasi, J.; Cossi, M.; Rega, N.; Millam, N. J.; Klene, M.; Knox, J. E.; Cross, J. B.; Bakken, V.; Adamo, C.; Jaramillo, J.; Gomperts, R.; Stratmann, R. E.; Yazyev, O.; Austin, A. J.; Cammi, R.; Pomelli, C.; Ochterski, J. W.; Martin, R. L.; Morokuma, K.; Zakrzewski, V. G.; Voth, G. A.; Salvador, P.; Dannenberg, J. J.; Dapprich, S.; Daniels, A. D.; Farkas, Ö.; Foresman, J. B.; Ortiz, J. V.; Cioslowski, J.; Fox, D. J. *Gaussian 09*, Revision C.01; Gaussian, Inc.: Wallingford, CT, 2009.
(48) (a) Becke, A. D. *J. Chem. Phys.* **1993**, *98*, 5648. (b) Perdew, J. P.; Wang, Y. *Phys. Rev. B* **1992**, *45*, 13244.
(49) (a) McLean, A. D.; Chandler, G. S. *J. Chem. Phys.* **1980**, *72*, 5639. (b) Raghavachari, K.; Binkley, J. S.; Seeger, R.; Pople, J. A. *J. Chem. Phys.* **1980**, *72*, 650. (c) Frisch, M. J.; Pople, J. A.; Binkley, J. S. *J. Chem. Phys.* **1984**, *80*, 3265. (d) Clark, T.; Chandrasekhar, J.; Spitznagel, G. W.; Schleyer, P. V. R. *J. Comput. Chem.* **1983**, *4*, 294.

(50) (a) Reed, A. E.; Weinstock, R. B.; Weinhold, F. *J. Chem. Phys.* **1985**, *83*, 735. (b) Reed, A. E.; Curtiss, L. A.; Weinhold, F. *Chem. Rev.* **1988**, *88*, 899.

(51) Cell parameters of $(TDAE)(S_4O_6)\cdot 2SO_2$: monoclinic, $P2_1/n$, a = 8.1540(13) Å, b = 15.851(3) Å, c = 18.524(3) Å, β = 99.853(2)°, V = 2358.9(7) Å^3, Z = 4, R_1 = 0.0785, R_2 = 0.0651. One SO_2 is severely disordered.

(52) Cell parameters of $(TDAE)(S_2O_7)\cdot SO_2$: monoclinic, $P2_1/n$, a = 11.187(3) Å, b = 14.253(4) Å, c = 11.975(4) Å, β = 98.283(4)°, V = 1889.5(10) Å^3, Z = 4, R_1 = 0.1281, R_2 = 0.1003.

dx.doi.org/10.1021/ic4022195 | *Inorg. Chem.* 2013, 52, 13651−13662